Multireference Ab Initio Quantum Mechanics/Molecular Mechanics Study on Intermediates in the Catalytic Cycle of Cytochrome $P450_{cam}$†

Ahmet Altun,‡ Devesh Kumar,‡ Frank Neese,§ and Walter Thiel*,‡

Max-Planck-Institut für Kohlenforschung, Kaiser-Wilhelm-Platz 1, D-45470 Mülheim an der Ruhr, Germany, and Institut für Physikalische und Theoretische Chemie, Universität Bonn, Wegelerstrasse 12, D-53115 Bonn, Germany

Received: March 10, 2008; Revised Manuscript Received: April 7, 2008

We have investigated the elusive reactive species of cytochrome $P450_{cam}$ (Compound I), the hydroxo complex formed during camphor hydroxylation, and the ferric hydroperoxo complex (Compound 0) by combined quantum mechanical/molecular mechanical (QM/MM) calculations, employing both density functional theory (DFT) and correlated ab initio methods. The first two intermediates appear multiconfigurational in character, especially in the doublet state and less so in the quartet state. DFT(B3LYP)/MM calculations reproduce the relative energies from correlated ab initio QM/MM treatments quite well, except for the splitting of the lowest $A_{1u}-A_{2u}$ radical states. The inclusion of dynamic correlation is crucial for the proper ab initio treatment of these intermediates.

I. Introduction

Cytochrome P450 enzymes are a ubiquitous monooxygenase superfamily of hemoproteins which are of vital importance for regulation of drug metabolism, detoxification of xenobiotics, and biosynthesis of metabolites.[1–3] They catalyze regio- and stereoselective C−H bond hydroxylation in many organic substances. For example, $P450_{cam}$ (CYP101) hydroxylates camphor at the C^5 position, leading to 5-*exo*-hydroxycamphor as the sole product.[4] Scheme 1 shows three key intermediates in the catalytic cycle of $P450_{cam}$. The ferric hydroperoxo complex called Compound 0 (Cpd 0) is the last species that is observed experimentally before the hydroxycamphor product. It can be converted to an oxyferryl−porphyrin cation called Compound I (Cpd I) which is generally believed to be the active oxidant of P450 enzymes. Cpd I of the thermostable cytochrome CYP119 was recently identified by its characteristic spectral features[5,6] and appeared to be relatively stable in kinetic studies,[6] whereas Cpd I of chloroperoxidase was found to be stable enough to be characterized by electron paramagnetic resonance and Mössbauer spectroscopy.[7,8] However, Cpd I of $P450_{cam}$ has never been detected, and its hydroxylation mechanism is still controversial.[1–11] The most common assumption is that Cpd I abstracts a hydrogen atom from camphor to yield a hydroxo intermediate (HYD) followed by a rebound that generates the product complex.[1–11]

Theoretical model studies (see ref 3 and references therein) as well as combined quantum mechanical/molecular mechanical (QM/MM) calculations,[12–16] which consider the complete $P450_{cam}$ enzyme, find barriers for the rate-determining H-abstraction reaction during camphor hydroxylation that seem too high to explain the elusiveness of Cpd I. Density functional theory (DFT) is the method of choice in almost all of these theoretical studies on high-valent metalloporphyrins and related molecules.[3] The question thus arises whether DFT is accurate enough for calculations of this kind, which calls for a careful calibration of DFT against high-level ab initio calculations.[17–22]

SCHEME 1: Key Intermediates in the Catalytic Cycle of P450 Enzymes

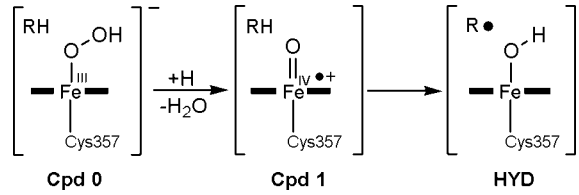

In this paper, we investigate the Cpd 0, Cpd I, and HYD intermediates of $P450_{cam}$ (see Scheme 1) by QM/MM calculations. The QM part is treated both with DFT and ab initio multireference configuration interaction (MR−CI) methods to allow for direct comparisons. In our previous QM/MM study on Cpd I of $P450_{cam}$ with MR−CI methods,[21] only the three singly occupied orbitals were included in the active space, which is sufficient for calculating the separation between the lowest doublet and quartet states. Here we use larger active spaces to assess the electronic structure of these species in more detail and to compute excitation energies to some lower-lying excited states. We examine doublet and quartet states in these intermediates but focus mainly on the quartet species. We do not address reaction energies and activation barriers presently, because an even-handed MR−CI treatment of all relevant species would be very demanding.

II. Computational Methods

The system used in this study for Cpd I and HYD corresponds to the snapX setup with protonated Asp297, as defined in refs 13–15. Cpd 0 is represented by the setup described in ref 23. Details of the adopted QM/MM methodology and protocols are given in refs 13–15 and 21. In the following, we only address some aspects relevant to the present study.

B3LYP/CHARMM geometry optimizations were performed by using the ChemShell[24] package and included all residues

† Part of the "Sason S. Shaik Festschrift".

* To whom correspondence should be addressed. E-mail: thiel@mpi-muelheim.mpg.de. Phone: +49-208-306-2150. Fax: +49-208-306-2996.
‡ Max-Planck-Institut für Kohlenforschung.
§ Universität Bonn.

10.1021/jp802092w CCC: $40.75
Published on Web 06/11/2008

TABLE 1: $^2A/^4A$ B3LYP/CHARMM Relative Energies (kcal/mol)

	R1/B1	R1/B′//R1/B1
Cpd I	0.0/0.1	0.0/0.3
HYD(III)[a]	9.0/10.1	6.7/7.8
HYD(IV)[a]	11.7/12.5	4.9/5.5
Cpd 0	0.0/8.3	0.0/7.5

[a] Energies relative to the ^2A state of Cpd I.

and water molecules that have atoms within a distance of 4 Å to any atom of the heme, coordinating Cys357, or camphor. All ab initio QM/MM calculations were carried out using the ORCA 2.4.44 program package[25] and R1/B1 B3LYP/CHARMM-optimized geometries. As in our previous work, QM region R1 consists of the heme (without side chains) and the axial ligands (SH and OOH for Cpd 0; SH and oxo plus propane to represent camphor in the case of Cpd I and HYD). Basis set B1 describes iron by a small-core effective core potential (ECP) together with the associated double-ζ quality LACVP basis[26] and all other atoms by 6-31G.[27] The ab initio R1/B′ QM/MM calculations employ the following basis (B′): Wachters all-electron basis set[28] in the contraction [8s6p4d2f] for iron; TZVP[29] for the six atoms coordinated to iron and for C^5; TZVPP[29] for H^{5exo}; SV[30] for the remaining atoms. The auxiliary basis set used is TZVPP/C for iron and TZV/C for the other atoms.[31] Throughout this paper, the oxidation state of iron will be specified in parenthesis (e.g., HYD(III)).

The zero-order wave function in all MR ab initio calculations was chosen to be the complete active-space self-consistent field (CASSCF)[32] wave function determined with quasi-restricted DFT(B3LYP) orbitals as initial guess; Hartree−Fock (HF) orbitals cannot be used for this purpose since HF calculations

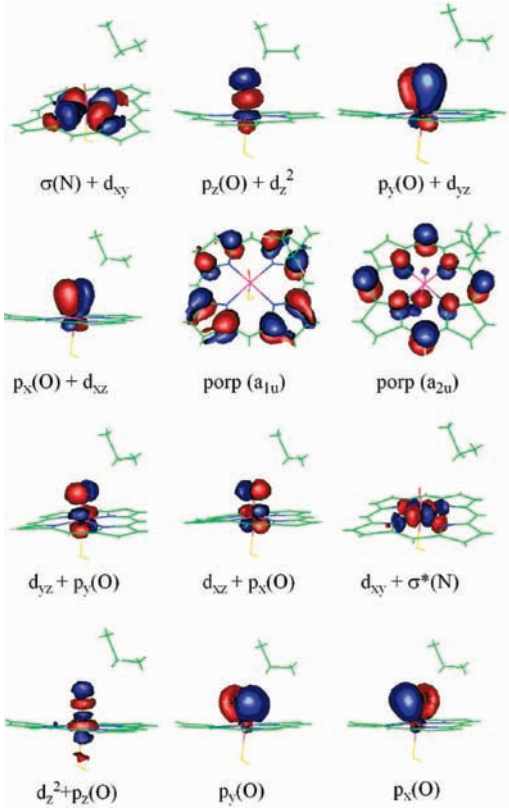

Figure 1. Active-space CASSCF(13,12) orbitals of Cpd I in the quartet state and their approximate descriptions.

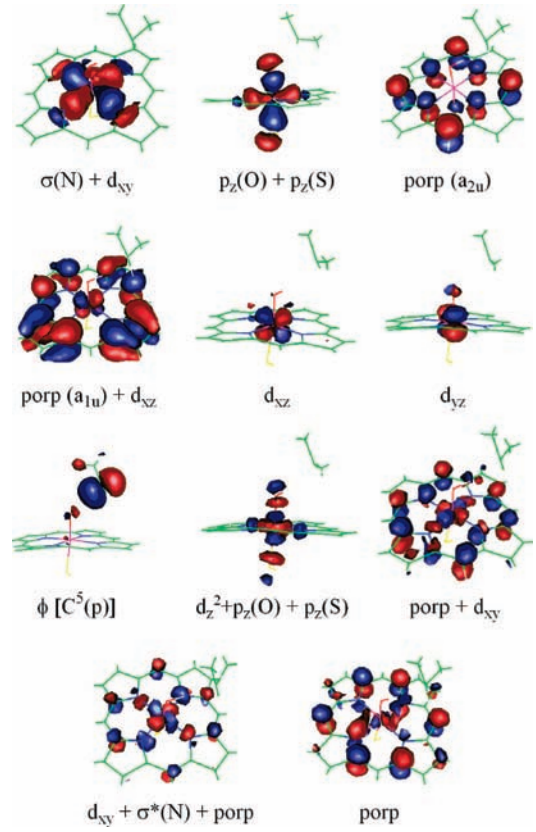

Figure 2. Active-space CASSCF(11,11) orbitals of HYD(IV) in the quartet state and their approximate descriptions.

predict the porphyrin a_{1u} and a_{2u} orbitals to be singly occupied for Cpd I and HYD. CASSCF captures the major part of the nondynamical correlation energy by mixing the active-space configurations at the full CI level. The subsequent ab initio MR−CI/MM calculations were carried out with a natural orbital iterative difference dedicated CI scheme (DDCI2)[33,34] that includes all single excitations as well as double excitations which involve either two holes in the occupied inactive orbitals or two particles in the inactive empty orbitals. The MR−Davidson correction (Q) for the effect of unlinked quadruple substitutions was applied to account for the fact that the DDCI2 method is not size consistent. Hence, the reported MR−CI/MM energies refer to DDCI2+Q.[34] To enhance computational efficiency without significant loss of accuracy, the ORCA thresholds T_{sel}, T_{pre}, and T_{nat} were set to 10^{-6} E_h, 10^{-4}, and 10^{-5}, respectively.[34,35] In a recent validation study on the model reaction $Fe^+ + H_2 \rightarrow FeO^+ + H_2O$, the DDCI2+Q approach was found to reproduce the energy profiles from higher-level ab initio MR methods quite well,[36] and it was therefore considered appropriate for the present study on larger related systems.

CAS calculations for Cpd I and HYD were performed both using a minimal active space of 3 electrons in 3 orbitals, and a large active space with 13 electrons in 12 orbitals for Cpd I and 11 electrons in 11 orbitals for HYD which was designed to properly describe the axial and equatorial ligand fields. These active spaces will be described in the next section in more detail. As a general guideline, we included all orbitals into the large active space that affect the computed relative energies significantly. For lower transition metal oxidation states, a second d shell (4d) is often essential for obtaining reliable correlated ab initio results.[37] Since this radial correlation effect becomes less pronounced as the metal oxidation state increases,[18] our active spaces do not include this unoccupied 4d shell at iron. It has

TABLE 2: Most Important DDCI2+Q Configuration State Functions of the Quartet State Cpd I in the Two Lowest Roots

root	ΔE (kcal/mol)	weight (%)	σ(N)	p_z(O)	p_y(O)	p_x(O)	a_{1u}	a_{2u}	d_{yz}	d_{xz}	d_{xy}	d_{z^2}	p_y(O)	p_x(O)
1	0.0	77.6	2	2	2	2	2	1	1	1	0	0	0	0
		2.0	2	1	2	1	2	1	2	1	0	1	0	0
		1.9	2	2	1	1	2	1	2	2	0	0	0	0
		1.8	2	1	1	2	2	1	1	2	0	1	0	0
		1.2	2	0	2	2	2	1	1	1	0	2	0	0
		1.0	2	2	2	1	2	1	2	1	0	0	0	0
		0.9	2	2	1	2	2	1	1	2	0	0	0	0
		0.6	1	2	2	2	2	1	1	1	1	0	0	0
		0.6	2	1	2	2	2	1	1	1	0	1	0	0
		0.5	2	2	2	2	1	0	1	1	0	0	1	1
		0.3	2	2	2	2	1	2	1	1	0	0	0	0
2	1.9	77.0	2	2	2	2	1	2	1	1	0	0	0	0
		2.0	2	1	2	1	1	2	2	1	0	1	0	0
		1.9	2	2	1	1	1	2	2	2	0	0	0	0
		1.8	2	1	1	2	1	2	1	2	0	1	0	0
		1.2	2	2	2	1	1	2	2	1	0	0	0	0
		1.1	2	0	2	2	1	2	1	1	0	2	0	0
		1.0	2	2	1	2	1	2	1	2	0	0	0	0
		0.7	2	1	2	2	1	2	1	1	0	1	0	0
		0.6	1	2	2	2	1	2	1	1	1	0	0	0
		0.4	2	2	2	2	0	1	1	1	0	0	1	1
		0.3	2	2	2	2	2	1	1	1	0	0	0	0

been noted previously for Fe^{III}(P)Cl and $[Fe(P)Cl]^+$ (P^{2-} = porphinato)[18] that CASSCF calculations erroneously predict the A_{1u} porphyrin radical states to be lower in energy than the A_{2u} radical states (by ca. 5 kcal/mol). It is thus possible that 1-root calculations with our large active space may not produce the lowest-energy configuration, and therefore we performed 6-root CASSCF calculations. This led to convergence for the quartet, but not for the doublet states. Hence, with the large active space, we can only present results for the quartet states for Cpd I and HYD. These complications are absent in Cpd 0 where the porphyrin a_{1u} and a_{2u} orbitals are doubly occupied both in the quartet and the doublet so that both spin states can be converged in 1-root calculations with a large active space comprising 13 electrons in 11 orbitals.

In all QM/MM calculations, an electronic embedding scheme[38] was applied, in which the fixed MM point charges are included in the one-electron Hamiltonian of the QM calculation and the QM/MM electrostatic interactions are evaluated from the QM electrostatic potential and the MM atomic charges. The electrostatic interactions between the QM region and the MM point charges were included in the QM energy. No cutoffs were introduced for the nonbonding MM and QM/MM interactions. Hydrogen link atoms[39] were used at the QM/MM boundary along with the charge shift model.[40]

III. Results

III.A. B3LYP/CHARMM Results. B3LYP/CHARMM optimizations indicate that Cpd I has almost degenerate quartet and doublet states with a slight preference (0.1−0.3 kcal/mol) for the doublet (see Table 1). Upon basis set extension from B1 to B′, HYD(III) [HYD(IV)] is stabilized by ca. 2 [7] kcal/mol relative to Cpd I, and the energy ordering changes such that HYD(IV) becomes more stable. The doublet ground state of HYD lies ca. 1 kcal/mol below the quartet for both oxidation states and both basis sets. Cpd 0 also has a doublet ground state, with a larger doublet−quartet gap of ca. 8 kcal/mol.

III.B. MR Ab Initio QM/MM Results. ***Compound I.*** The minimal active space for Cpd I consists of the three singly occupied orbitals, i.e., the antibonding π^*_{xz} and π^*_{yz} molecular orbitals (MOs) built from the iron d_{xz}/d_{yz} and oxygen p_x/p_y orbitals, and the porphyrin a_{2u} orbital. CASSCF(3,3)-DDCI2+Q/MM calculations yield a doublet−quartet splitting of −1.8 kcal/mol in state-specific calculations at separately optimized geometries and of −1.2 kcal/mol in state-averaged calculations at the quartet state geometry. The previous[21] CAS(3,3) DDCI2+Q/MM result of −0.1 kcal/mol on top of spin-restricted DFT orbitals generated with the BP86 functional is closer to the B3LYP/CHARMM result of −0.3 kcal/mol (see Table 1). The previous calculations[21] differ from the present ones in the choice of orbitals for the DDCI2+Q treatment [DFT(BP86) vs CASSCF] and in the use of tighter ORCA thresholds (see section II) which affects the relative spin state energies by ca. 1 kcal/mol in this case (see also footnote 60 of ref 21).

The CASSCF(3,3) calculations for Cpd I predict a multiconfigurational doublet state, with major contributions from three configurations with the following occupancies of $\pi^*_{xz}\pi^*_{yz}a_{2u}$: 210 (38%), 012 (30%), and 111 (22%). The CAS(3,3) DDCI2+Q Mulliken spin populations on FeO (1.35 e), sulfur (−0.03 e), and pyrrolic nitrogens (average, −0.04 e) are considerably lower than the B3LYP values (2.14, −0.24, and −0.18 e, respectively). Hence, broken-symmetry DFT treatments cannot be used to calculate spin-dependent properties of doublet Cpd I without applying a spin projection scheme. The spin populations of the quartet state with a dominant 111 configuration (90%) are analogous in DDCI2+Q (1.99, 0.07, and 0.14 e) and B3LYP (2.05, 0.21, and 0.16 e).

It should be noted that the quartet 111 configuration will be lower in energy than the corresponding doublet 111 configuration built from the same set of MOs. The doublet can be stabilized by mixing in the ionic 210 and 120 configurations (not available in the quartet case), and it depends on the extent of this admixture whether the doublet becomes the ground state. This is the case in our present and previous[21] CASSCF(3,3)-DDCI2+Q calculations, even though the doublet and quartet were more nearly degenerate previously. The actual numerical results depend on subtle factors (see above), but in a qualitative sense it is the multiconfigurational character of the doublet (i.e., the mixing between the 111, 210, and 120 configurations) which provides the mechanism for bringing the doublet below the quartet (when using symmetry-adapted rather than symmetry-broken MOs).

TABLE 3: Most Important DDCI2+Q Configuration State Functions in the Lowest Six Quartet States of HYD

root	ΔE (kcal/mol)	weight (%)	σ(N)	p_z(O, S)	a_{2u}	a_{1u}	d_{xz}	d_{yz}	ϕ	d_{z^2}	porp	d_{xy}	Porp
1	0.00	67.6	2	2	2	2	1	1	1	0	0	0	0
		15.5	2	2	2	1	2	1	1	0	0	0	0
		2.2	2	2	2	1	1	1	1	1	0	0	0
		0.5	2	2	1	2	0	1	1	0	1	1	0
		0.4	2	2	2	2	1	1	1	0	1	0	0
		0.3	2	0	2	2	1	1	1	2	0	0	0
		0.3	2	2	2	2	1	1	1	0	0	1	0
2	2.1	82.3	2	2	1	2	2	1	1	0	0	0	0
		1.2	2	2	2	1	1	2	1	0	0	0	0
		1.0	2	2	1	1	2	1	1	1	0	0	0
		0.5	2	2	0	2	1	1	1	0	1	1	0
		0.4	2	0	1	2	2	1	1	2	0	0	0
		0.4	2	2	1	2	2	1	1	0	1	0	0
		0.4	2	2	1	2	2	1	1	0	0	1	0
3	7.6	82.8	2	2	2	1	1	2	1	0	0	0	0
		1.2	2	2	1	2	2	1	1	0	0	0	0
		0.6	2	2	1	1	0	2	1	0	1	1	0
		0.5	2	2	2	1	1	2	1	1	0	0	0
		0.4	2	0	2	1	1	2	1	2	0	0	0
		0.4	2	2	2	1	1	2	1	0	1	0	0
		0.3	2	2	2	1	1	0	1	0	0	0	2
		0.3	2	2	0	1	1	2	1	0	2	0	0
		0.3	2	2	2	1	1	2	1	0	0	1	0
4	12.8	66.7	2	2	1	1	2	1	1	1	0	0	0
		16.3	2	2	1	2	1	1	1	1	0	0	0
		1.5	2	2	1	2	2	1	1	0	0	0	0
		0.6	2	2	0	1	1	1	1	1	1	1	0
		0.4	2	2	2	1	2	1	1	0	0	0	0
		0.4	2	2	1	2	2	1	0	1	0	0	0
		0.4	2	2	1	1	2	1	2	0	0	0	0
		0.4	2	2	1	1	0	1	1	1	2	0	0
		0.4	2	2	1	1	2	1	1	1	1	0	0
		0.3	2	2	1	1	0	1	1	1	0	2	0
		0.3	1	2	1	1	2	1	1	1	0	0	1
		0.3	2	2	1	1	2	1	1	1	0	1	0
5	14.2	82.0	2	2	2	1	1	1	1	1	0	0	0
		1.7	2	2	2	2	1	1	1	0	0	0	0
		0.9	2	2	2	1	1	1	2	0	0	0	0
		0.7	2	2	1	1	0	1	1	1	1	1	0
		0.6	2	2	2	2	1	1	0	1	0	0	0
		0.5	2	2	2	1	2	1	1	0	0	0	0
		0.5	1	2	2	1	1	1	1	1	0	0	1
		0.4	2	2	2	1	1	1	1	1	1	0	0
		0.4	2	2	2	1	1	1	1	1	0	1	0
		0.3	2	2	0	1	1	1	1	1	2	0	0
6	14.7	51.6	2	2	2	1	1	1	1	1	0	0	0
		17.5	2	2	2	0	2	1	1	1	0	0	0
		16.9	2	2	2	2	0	1	1	1	0	0	0
		0.7	2	2	1	1	0	1	1	1	1	1	0
		0.5	2	2	2	1	1	1	1	1	1	0	0
		0.4	2	2	2	1	1	1	1	1	0	1	0
		0.3	1	2	2	1	1	1	1	1	0	0	1

In addition to the three singly occupied orbitals, the large active space for Cpd I includes the bonding π_{xz} and π_{yz} MOs of the iron−oxo moiety, the axial σ and σ^* MOs composed of iron d_{z^2}, oxygen p_z, and sulfur p_z orbitals, the equatorial σ and σ^* MOs derived from iron d_{xy} and nitrogen orbitals, the porphyrin a_{1u} orbital, and the strongly correlating unoccupied oxygen $3p_x$ and $3p_y$ orbitals. The iron d_{xy} and the sulfur lone-pair p orbital were not put into the active space because doing so in test calculations did not affect the CASSCF excitation energies significantly. The 6-root CASSCF(13,12) orbitals of Cpd I in the quartet state are shown in Figure 1. The calculations yield roots that contain strong contributions from configurations with singly occupied a_{1u} and a_{2u} porphyrin orbitals, respectively. The lowest "A_{1u} root" lies 6.3 kcal/mol below the lowest "A_{2u} root" at the CASSCF/MM level, which is reversed at the DDCI2+Q/MM level where the "A_{2u} root" is more stable by 1.9 kcal/mol. Hence, dynamic correlation is crucial for obtaining the correct ground state. As B3LYP accounts for dynamic correlation, it is not surprising that the lowest-energy Kohn−Sham determinant contains singly occupied π^*_{xz}, π^*_{yz}, and a_{2u} orbitals as in DDCI2+Q. The DDCI2+Q configuration state functions (CSF) with weights of more than 0.3% are given in Table 2 for the lowest two roots. The DDCI2+Q/MM excitation energies to the other four roots, which are mainly made up of configurations that have one electron in each of the d_{xy}, d_{xz} (or d_{yz}), and a_{2u} (or a_{1u}) orbitals, are 31−35 kcal/mol. If the equatorial σ and σ^* MOs are not included in the active space, the excitation energy to the first accessible state remains essentially the same (1.9 vs 1.6 kcal/mol) but the energies of the other four roots are underestimated by ca. 10 kcal/mol as the corresponding

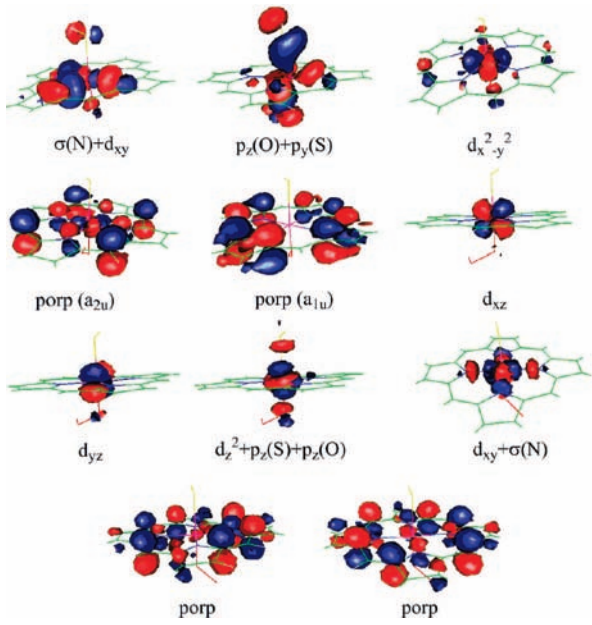

Figure 3. Active-space CASSCF(13,11) orbitals of Cpd 0 from a spin-averaged treatment and their approximate descriptions (see text).

excitations involve the iron d_{xy} orbital (see Figure 1, notation according to ref 3 throughout this paper).

In the CASSCF(13,12)-DDCI2+Q wave function of the two lowest quartet states (Table 2), the most important configuration in the ground state (weight 78%) has one electron in each of π^*_{xz}, π^*_{yz}, and a_{2u} orbitals, in agreement with the CASSCF(3,3) and B3LYP calculations. Enlarging the active space from CAS(3,3) to CAS(13,12) reduces the weight of the dominant configuration by ca. 12%, indicating some multiconfigurational character also for the quartet ground state. The first excited quartet state is characterized by a configuration with one electron in each of π^*_{xz}, π^*_{yz}, and a_{1u} orbitals (weight 77%). Since it lies only 1.9 kcal/mol above the ground state (according to the DDCI2+Q/MM results), it might even play a role in the reactivity of Cpd I. By contrast, TDDFT(B3LYP)/MM calculations predict an energy of 12.3 kcal/mol for this "A_{1u} root" which should then be hardly accessible in reactions. The Mulliken spin populations of the quartet ground state are qualitatively comparable in DDCI2+Q/MM (FeO, 2.02 e; S, 0.00 e; N, −0.02 e; porphyrin, 0.97 e) and B3LYP/MM (FeO, 2.05 e; S, 0.21 e; N, 0.16 e; porphyrin, 0.74 e), as expected since the same configuration is dominant in both treatments.

Hydroxo Intermediate HYD. The minimal active space for HYD(IV) contains the three singly occupied orbitals, i.e., the iron d_{xz} and d_{yz} orbitals and the radical p orbital of the C^5 atom of camphor (abbreviated as ϕ). CASSCF(3,3)-DDCI2+Q/MM calculations yield a doublet−quartet splitting of −2.0 kcal/mol in state-specific calculations at separately optimized geometries and of −1.8 kcal/mol in state-averaged calculations at the quartet state geometry, similar to the B3LYP/MM result of −0.6 kcal/mol (see Table 1). The doublet−quartet splitting of HYD(III) species is similar in CASSCF(3,3)-DDCI2+Q/MM (−2.4 kcal/mol in state-specific calculations at separate geometries; −0.6 kcal/mol in state-averaged calculations at the quartet state geometry; active space: $d_{xz} + \phi$, d_{yz}, and $\phi + \pi^*_{xz}$ orbitals) and B3LYP/MM (−1.1 kcal/mol, see Table 1). The ab initio calculations for the hydroxo complex again give a multiconfigurational doublet state, as in the case of Cpd I. For the HYD(IV) reference function of the doublet, the dominant CSFs have the following occupancies of the d_{xz}, d_{yz}, and ϕ orbitals: 210 (45%), 012 (29%), and 111 (23%); hence, the ferryl configuration contributes less than the ferric configuration. For the HYD(III) reference function of the doublet, the dominant CSFs show the following occupancies of the $d_{xz} + \phi$, d_{yz}, and $\phi + \pi^*_{xz}$ orbitals: 210 (49%), 012 (41%), and 111(2%). In view of the multiconfigurational character of the doublet in both oxidation states, it is remarkable that the relative spin state energies from B3LYP/MM agree with the ab initio QM/MM results within 2 kcal/mol.

The CASSCF(3,3)-DDCI2+Q Mulliken spin populations of FeO, S, camphor, porphyrin, and pyrrolic nitrogens for the doublet state of HYD(III) {0.98, 0.00, −0.14, 0.16, and 0.02 e} and HYD(IV) {1.40, −0.04, −0.32, −0.04, and −0.09 e} are significantly different from the B3LYP values for HYD(III) {1.15, −0.16, 0.88, −0.86 e, and −0.18 e} and for HYD(IV) {2.15, −0.11, −0.91, −0.14, and −0.05 e}, which again emphasizes the inappropriateness of broken-symmetry DFT solutions for spin-dependent properties. As the CAS(3,3) quartet wave function is dominated by the 111 configuration (>90%), the DDCI2+Q Mulliken spin populations for HYD(IV) {2.16, −0.07, 0.99, −0.07, and −0.02 e} and for HYD(III) {0.99, 0.03, 0.99, 0.99, and 0.13 e} are analogous to the B3LYP results for HYD(IV) {2.27, −0.08, 0.96, −0.14, and −0.05 e} and for HYD(III) {1.08, 0.17, 0.96, 0.79, and 0.16 e}, respectively.

In addition to the three singly occupied orbitals, the large active space for HYD(IV) includes the axial and equatorial σ and σ^* MOs (as in the case of Cpd I), the porphyrin a_{1u} and a_{2u} orbitals, and two correlating unoccupied porphyrin orbitals. The 6-root CASSCF(11,11) orbitals of HYD(IV) in the quartet state are shown in Figure 2. The lowest "A_{1u} root" is again 5.3 kcal/mol more stable than the next lowest root at the CASSCF/MM level. The inclusion of dynamic correlation in the DDCI2+Q/MM calculations reverses this order and makes the "A_{2u} root" the lowest one in energy, as in case of B3LYP/MM.

The most important contribution to the quartet ground-state wave function of HYD (see Table 3) comes from an Fe(IV) configuration with a weight of 68% (singly occupied orbitals: d_{xz}, d_{yz}, and ϕ), but there is also a notable contribution of 16% from an Fe(III) configuration (singly occupied orbitals: a_{1u}, d_{yz}, and ϕ). The next quartet state (at 2.1 kcal/mol) is mainly of Fe(III) character (configuration with singly occupied orbitals a_{2u}, d_{yz}, and ϕ: weight of 82%). Although both these HYD(III) and HYD(IV) species are to some extent multiconfigurational, the B3LYP-based estimates of their separation (adiabatic QM/MM energy difference of 2.7 kcal/mol; vertical QM energy difference of 3.2 kcal/mol at HYD(IV) geometry) agree well with the vertical DDCI2+Q/MM energy difference (2.1 kcal/mol).

The second excited quartet state of HYD, with an excitation energy of 7.6 kcal/mol, corresponds to an "A_{1u} root" of HYD(III) character (leading configuration with singly occupied orbital a_{1u}, d_{xz}, and ϕ, weight of 83%). The DDCI2+Q/MM excitation energies to the other three roots, which involve a_{1u} (or d_{xz}) → d_{z^2} excitations, are very similar to each other (between 12.8 and 14.7 kcal/mol, see Table 3). The third excited state of HYD (at 12.8 kcal/mol) features $a_{1u} \rightarrow d_{z^2}$ (67%) and $d_{xz} \rightarrow d_{z^2}$ (16%) excitations in HYD(III) configurations with single occupation of a_{2u}. The next one (at 14.2 kcal/mol) involves $a_{1u} \rightarrow d_{z^2}$ (82%) excitations on HYD(IV). The fifth one (at 14.7 kcal/mol) is characterized by an $a_{1u} \rightarrow d_{z^2}$ (52%) excitation on HYD(IV), with additional contributions from a $d_{xz} \rightarrow d_{z^2}$ (15%) single excitation and from double excitations from a_{1u} to d_{z^2} and d_{xz} (18%).

TABLE 4: Most Important DDCI2+Q Configuration State Functions of the Doublet (^{2}A) and Quartet (^{4}A) State Cpd 0

state	weight (%)	σ(N)	p_z(O, S)	$d_{x^2-y^2}$	A_{2u}	a_{1u}	d_{xz}	d_{yz}	d_{z^2}	d_{xy}	porp	porp
^{2}A	86.5	2	2	2	2	2	2	1	0	0	0	0
	0.8	2	2	1	2	2	1	1	0	0	1	1
	0.4	2	2	2	2	2	0	1	0	0	2	0
^{4}A	86.8	2	2	2	2	2	1	1	1	0	0	0
	1.5	2	2	2	1	1	1	1	1	0	1	1
	0.4	2	2	1	2	2	1	1	1	1	0	0
	0.4	2	2	2	2	0	1	1	1	0	0	0
	0.4	2	2	2	2	0	1	1	1	0	0	2

Compound 0. The minimal active space for the doublet state of Cpd 0 consists of three electrons in the two π^*_{xz} and π^*_{yz} antibonding MOs (doubly and singly occupied, respectively, in the leading ground-state configuration), whereas the minimal description of the quartet state requires three electrons in the three antibonding π^*_{xz}, π^*_{yz}, and $\sigma^*_{z^2}$ MOs (all singly occupied). Separate CAS-based calculations with these minimal spaces are unbalanced and do not yield reliable doublet−quartet splittings for Cpd 0. We thus consider only a common large active space with 13 electrons in 11 orbitals. In addition to the antibonding π^*_{xz}, π^*_{yz}, and $\sigma^*_{z^2}$ MOs (see above), it contains the axial σ MO, the equatorial σ and σ^* MOs, the porphyrin a_{1u} and a_{2u} orbitals, and two correlating unoccupied porphyrin orbitals (as in the case of HYD) as well as the doubly occupied iron $d_{x^2-y^2}$ (δ) orbital. The active-space (13,11) orbitals of Cpd 0 from a state-averaged treatment are shown in Figure 3. State-specific calculations yield analogous active-space orbitals with more pronounced mixing between nearly degenerate doubly occupied MOs. Contrary to the situation in Cpd I and HYD, the wave functions for the lowest doublet and quartet states of Cpd 0 are always dominated by the leading CASSCF configuration so that 1-root calculations are sufficient for each spin state (which converge without problems).

CAS(13,11) DDCI2+Q calculations yield a doublet−quartet splitting of 10.6 kcal/mol in state-specific calculations at separately optimized geometries and of 3.7 kcal/mol in state-averaged calculations at the quartet state geometry. These values bracket the B3LYP doublet−quartet splitting of 7.5 kcal/mol (Table 1) which is closer to the former DDCI2+Q value. The CAS(13,11) DDCI2+Q spin populations (doublet/quartet values) on the FeOOH (1.02 e/2.91 e), SH (−0.01 e/0.06 e), and porphyrin (−0.01 e/0.03 e) moieties are consistent with the corresponding B3LYP values (FeOOH, 1.09 e/2.93 e; SH, −0.03 e/0.15 e; porphyrin, −0.06 e/−0.06 e). This is not surprising since the leading configuration corresponds to the Kohn−Sham determinant in both states, with a weight of 86−87% (compared with less than 2% for the next most important configurations, see Table 4). The lowest doublet and quartet state of Cpd 0 are thus of single-reference character, and they are qualitatively well described by the leading monoradicaloid and triradicaloid configurations, respectively.

IV. Discussion and Conclusions

Compound 0, Compound I, and the hydroxo intermediate in the catalytic cycle of cytochrome $P450_{cam}$ have been studied by B3LYP/CHARMM and correlated ab initio CASSCF-DDCI2+Q/CHARMM calculations. According to the ab initio results, all species have a doublet ground state which has a pronounced multiconfigurational character in the case of Cpd I and HYD. The B3LYP/CHARMM calculations also give a doublet ground state and reproduce the doublet−quartet splitting well (typically within ca. 2 kcal/mol). However, the broken-symmetry DFT solution for the doublet Cpd I and HYD does not capture the multiconfigurational nature of this state and can thus not be used for the calculation of any spin-dependent property without applying a spin projection scheme.

The CASSCF calculations with the larger active space for Cpd I [CAS(13,12)] and for HYD [CAS(11,11)] converged only for the quartet state. For both species, the lowest CASSCF root corresponds to a state with A_{1u} porphyrin radical character. Inclusion of dynamic correlation in 6-root CASSCF-DDCI2+Q calculations reverses the order of states such that the most stable quartet state has A_{2u} character. Dynamic correlation is thus crucial for obtaining the correct lowest-energy quartet state. Similar findings have been reported in porphyrin model systems with an axial Cl ligand,[18] where CASSCF (CASPT2) calculations gave an A_{1u} (A_{2u}) ground state. We conclude that 1-root multireference ab initio calculations on top of CASSCF orbitals may yield erroneous results for heme systems containing porphyrin radicals and that several roots should always be computed in such calculations. This caveat does not apply to systems with a neutral porphyrin ring, such as the previously studied oxy- and oxo-heme complexes,[18,41] where the porphyrin a_{1u} and a_{2u} orbitals are both doubly occupied. Likewise, and for the same reason, Cpd 0 can be described with 1-root calculations which converge for both spin states with the large active space [CAS(13,11)], leading to solutions that are dominated a single configuration (i.e., the Kohn−Sham determinant).

Both for Cpd I and HYD, the lowest-energy states from the B3LYP/MM and CASSCF-DDCI2+Q/MM calculations with basis B′ always correspond to ferryl [Fe(IV)] A_{2u} radical states. The computed $A_{1u}-A_{2u}$ splitting between the lowest quartet states of Cpd I is only 1.9 kcal/mol at the CASSCF(13,12)-DDCI2+Q/MM level, significantly smaller than the value of 12.3 kcal/mol from TDDFT(B3LYP)/MM calculations. In the case of HYD, the DFT and ab initio treatments both yield small values of 2 kcal/mol or less for this splitting.

In summary, the present comparisons show that B3LYP reproduces the relative spin state energies and excitation energies from the correlated ab initio treatment quite well (except for the $A_{1u}-A_{2u}$ splitting in Cpd I), in spite of the multiconfigurational character of some of the states considered (especially the doublet states). Further calibration studies with comparisons against high-level multireference ab initio results are desirable to check the performance of DFT (and particularly B3LYP) for other electronically demanding species in heme chemistry.

Acknowledgment. This work was supported by the Volkswagenstiftung (Grant I/80540).

References and Notes

(1) (a) Ortiz de Montellano, P. R. Ed. *Cytochrome P450: Structure, Mechanisms, and Biochemistry*, 2nd ed.; Plenum Presss: New York, 1995. (b) Ortiz de Montellano, P. R. Ed. *Cytochrome P450: Structure, Mechanism, and Biochemistry*, 3rd ed.; Kluwer Academic/Plenum Publishers: New York, 2004.

(2) Denisov, I. G.; Makris, T. M.; Sligar, S. G.; Schlichting, I. *Chem. Rev.* **2005**, *105*, 2253.

(3) Shaik, S.; Kumar, D.; de Visser, S. P.; Altun, A.; Thiel, W. *Chem. Rev.* **2005**, *105*, 2279.

(4) Mueller, E. J.; Lioda, P. J.; Sligar, S. G. In *Cytochrome P450: Structure, Mechanism, and Biochemistry*, 2nd ed.; Ortiz de Montellano, P. R. Ed.; Plenum Press: New York, 1995; Vol. 2, Chapter 3.

(5) (a) Egawa, T.; Shimada, H.; Ishimura, Y. *Biochem. Biophys. Res. Commun.* **1994**, *201*, 1464. (b) Kellner, D. G.; Hung, S.-C.; Weiss, K. E.; Sligar, S. G. *J. Biol. Chem.* **2002**, *277*, 9641. (c) Spolitak, T.; Dawson, J. H.; Ballou, D. P. *J. Biol. Chem.* **2005**, *280*, 20300.

(6) Newcomb, M.; Zhang, R.; Chandrasena, R. E. P.; Halgrimson, J. A.; Horner, J. H.; Makris, T. M.; Sligar, S. G. *J. Am. Chem. Soc.* **2006**, *128*, 4580.

(7) Rutter, R.; Hager, L. P.; Dhonau, H.; Hendrich, M.; Valentine, M.; Debrunner, P. *Biochemistry* **1984**, *23*, 6809.

(8) Kim, S. H.; Perera, R.; Hager, L. P.; Dawson, J. H.; Hoffman, B. M. *J. Am. Chem. Soc.* **2006**, *128*, 5598.

(9) Groves, J. T.; Watanabe, Y. *J. Am. Chem. Soc.* **1988**, *110*, 8443.

(10) Dunford, H. B. *Heme Peroxidases*; Wiley-VCH: New York, 1999.

(11) Messerschmidt, A., Huber, R., Poulos, T. L., Wieghardt, K. Eds. *Handbook of Metalloproteins*; John-Wiley and Sons: New York, 2001; Vol. 1.

(12) Schöneboom, J. C.; Cohen, S.; Lin, H.; Shaik, S.; Thiel, W. *J. Am. Chem. Soc.* **2004**, *126*, 4017.

(13) Altun, A.; Guallar, V.; Friesner, R. A.; Shaik, S.; Thiel, W. *J. Am. Chem. Soc.* **2006**, *128*, 3924.

(14) Altun, A.; Shaik, S.; Thiel, W. *J. Comput. Chem.* **2006**, *27*, 1324.

(15) Altun, A.; Shaik, S.; Thiel, W. *J. Am. Chem. Soc.* **2007**, *129*, 8978.

(16) Zheng, J. J.; Altun, A.; Thiel, W. *J. Comput. Chem.* **2007**, *28*, 2147.

(17) Koch, W.; Holthausen, M. C. *A Chemist's Guide to Density Functional Theory*; Wiley-VCH: New York, 2000.

(18) Ghosh, A.; Persson, B. J.; Taylor, P. R. *J. Biol. Inorg. Chem.* **2003**, *8*, 507.

(19) Ghosh, A.; Taylor, P. R. *Curr. Opin. Chem. Biol.* **2003**, *7*, 113.

(20) Neese, F. *J. Biol. Inorg. Chem.* **2006**, *100*, 716.

(21) Schöneboom, J. C.; Neese, F.; Thiel, W. *J. Am. Chem. Soc.* **2005**, *127*, 5840.

(22) Radon, M.; Broclawik, E. *J. Chem. Theory Comput.* **2007**, *3*, 728.

(23) Zheng, J.; Wang, D.; Thiel, W.; Shaik, S. *J. Am. Chem. Soc.* **2006**, *128*, 13204.

(24) (a) ChemShell is a modular QM/MM program developed in the European QUASI project under the coordination of P. Sherwood. See: http://www.chemshell.org. (b) Sherwood, P.; de Vries, A. H.; Guest, M. F.; Schreckenbach, G.; Catlow, C. R. A.; French, S. A.; Sokol, A. A.; Bromley, S. T.; Thiel, W.; Turner, A. J.; Billeter, S.; Terstegen, F.; Thiel, S.; Kendrick, J.; Rogers, S. C.; Casci, J.; Watson, M.; King, F.; Karlsen, E.; Sjovoll, M.; Fahmi, A.; Schäfer, A.; Lennartz, C. *J. Mol. Struct. (THEOCHEM)* **2003**, *632*, 1.

(25) Neese, F. *ORCA*, an ab initio, DFT and semiempirical electronic structure package, version 2.4, revision 44; Max-Planck-Institut für Bioanorganische Chemie: Mülheim an der Ruhr, Germany, 2005.

(26) Hay, J. P.; Wadt, W. R. *J. Chem. Phys.* **1985**, *82*, 299.

(27) (a) Ditchfield, R.; Hehre, W. J.; Pople, J. A. *J. Chem. Phys.* **1971**, *54*, 724. (b) Hehre, W. J.; Ditchfield, R.; Pople, J. A. *J. Chem. Phys.* **1972**, *56*, 2257. (c) Hariharan, P. C.; Pople, J. A. *Theor. Chim. Acta* **1973**, *28*, 213. (d) Clark, T.; Chandrasekhar, J.; Spitznagel, G. W.; Schleyer, P. v. R. *J. Comput. Chem.* **1983**, *4*, 294.

(28) (a) Wachters, A. J. H. *J. Chem. Phys.* **1970**, *52*, 1033. (b) Hay, P. J. *J. Chem. Phys.* **1977**, *66*, 4377. (c) Bauschlicher, C. W., Jr.; Langhoff, S. R.; Barnes, L. A. *J. Chem. Phys.* **1989**, *91*, 2399.

(29) (a) Ahlrichs, R.; May, K. *Phys. Chem. Chem. Phys.* **2000**, *2*, 943. (b) Schäfer, A.; Huber, C.; Ahlrichs, R. *J. Chem. Phys.* **1994**, *100*, 5829.

(30) Schäfer, A.; Horn, H.; Ahlrichs, R. *J. Chem. Phys.* **1992**, *97*, 2571.

(31) (a) The auxiliary basis sets were obtained from the TURBOMOLE basis set library under ftp.chemie.uni-karlsruhe.de/pub/cbasen. (b) Eichkorn, K.; Weigend, F.; Treutler, O.; Ahlrichs, R. *Theor. Chem. Acc.* **1997**, *97*, 119. (c) Weigend, F.; Häser, M. *Theor. Chem. Acc.* **1997**, *97*, 331.

(32) Roos, B. O.; Taylor, P. R. *Chem. Phys.* **1980**, *48*, 157.

(33) Miralles, J.; Castell, O.; Caballol, R.; Malrieu, J. P. *Chem. Phys.* **1993**, *172*, 33.

(34) Neese, F. *J. Chem. Phys.* **2003**, *119*, 9428.

(35) Wanko, M.; Hoffman, M.; Strodel, P.; Koslowski, A.; Thiel, W.; Neese, F.; Frauenheim, T.; Elstner, M. *J. Phys. Chem. B* **2005**, *109*, 3606.

(36) Altun, A.; Neese, F.; Thiel, W. **2008**, to be submitted for publication.

(37) Roos, B. O.; Andersson, K.; Fülscher, M. P.; Malmqvist, P.-A.; Serrano-Andrés, L.; Pierloot, K.; Merchán, M. *Adv. Chem. Phys.* **1996**, *93*, 219.

(38) Bakowies, D.; Thiel, W. *J. Phys. Chem.* **1996**, *100*, 10580.

(39) Antes, I.; Thiel, W. *Hybrid Quantum Mechanical and Molecular Mechanical Methods*; Gao, J. Ed.; ACS Symposium Series 712; American Chemical Society: Washington, DC, 1998; p 50.

(40) de Vries, A. H.; Sherwood, P.; Collins, S. J.; Rigby, A. M.; Rigutto, M.; Kramer, G. J. *J. Phys. Chem. B* **1999**, *103*, 6133.

(41) Yamamoto, S.; Teraoka, J.; Kashiwagi, H. *J. Chem. Phys.* **1988**, *88*, 303.

JP802092W